JOURNAL OF MATERIALS SCIENCE 23 (1988) 3031–3040

Anisotropy of foams

A. T. HUBER, L. J. GIBSON
Department of Civil Engineering, Massachusetts Institute of Technology, Cambridge, Massachusetts 02139, USA

Cellular materials are often anisotropic, i.e. their properties depend on the direction in which they are measured. In this paper, we model the mechanical behaviour of anisotropic foams to describe the ratio of foam properties in two orthogonal directions in terms of the mean intercept lengths of the cells. Experimental measurements of the mean cell intercept lengths and of the mechanical properties of two polyurethane foams indicate that the model describes anisotropy well.

1. Introduction

Cellular materials are widespread. In nature they occur, for example, as wood, cancellous bone and cork. And man makes his own cellular materials in the form of honeycombs and foams. The size of the cells in such materials often varies with direction and because of this, the properties of the material, too, depend on direction: the material is said to be anisotropic. Honeycomb-like materials with prismatic cells are often strongly anisotropic: the Young's modulus of low-density woods, for instance, can be up to 100 times larger along the grain than across it. Foams, too, are usually anisotropic, although less strongly so: the Young's modulus of a foam usually varies with direction by less than a factor of 4.

Polymer foams made by pouring the polymer plus a hardener and a foaming agent into a mould (so that it rises like a loaf of bread) usually have cells which are elongated in the rise direction and equiaxed in the plane normal to it, giving an axisymmetric structure. The anisotropy in cell shape can conveniently be measured by the ratio of the mean intercept length in the rise direction to that in the perpendicular plane; we call this the shape-anisotropy ratio, R. The value of R for polymer foams is typically about 1.3 (Figs 1a, b); it varies from 1 for an isotropic foam to 10 or more for one which is very anisotropic, like the pumice shown in Fig. 1c. Many foams are approximately axisymmetric, but some (depending on how they are made) are orthotropic: then all three principal dimensions of the cell differ, and two values of R are needed to characterize it.

In this paper we model the mechanical properties of a foam in terms of the shape-anisotropy ratio, R. The results of the model are compared with measurements of cell size and mechanical properties for flexible and rigid polyurethane foams; they describe anisotropy well.

2. Literature

The mechanical behaviour of isotropic cellular materials has been modelled by identifying and analysing the mechanism of deformation determining each property. In particular, it has been found that the linear elastic behaviour of cellular materials is related to bending of the cell walls [1–5]; that elastic collapse in compression is related to cell wall buckling [4, 6, 7]; that plastic yield is related to the formation of plastic hinges in the cell walls [4]; that brittle crushing is related to the compressive fracture of cell walls [5]; and that the fracture toughness is related to the tensile fracture of cell walls [8]. Recently, a comprehensive model for the mechanical behaviour of isotropic foams has been developed [9].

Less attention has been directed at understanding anisotropic cellular materials. The mechanical properties of simple honeycomb-like materials made up of an array of prismatic hexagonal cells can be related to the cell geometry, the volume fraction of solids and the cell wall properties in an exact way [10, 11]. The degree of anisotropy in the mecanical properties can then easily be found in terms of the cell geometry. Foams, with their more complicated geometry, are more difficult to model. Harrigan and Mann [12] have shown that the shape of the cells can be characterized by an anisotropy tensor. Previous attempts to describe the anisotropy in Young's modulus have assumed that it is determined by the uniaxial deformation of the cell walls [12–16]. The difficulty with these models is that it is the bending rather than the uniaxial deformation of the cell walls which dominate the linear elastic behaviour of foams. We now model anisotropy in the moduli based on bending deformations in the cell walls, and extend the model to the elastic, plastic and brittle collapse stresses and to the fracture toughness.

3. Analysis

Typical compressive stress–strain curves for axisymmetric flexible and rigid polyurethane foams are given in Fig. 2. The foams were loaded in the rise direction (X_3) and in two perpendicular directions in the plane normal to the rise direction (X_1 and X_2). The Young's modulus and the elastic and plastic collapse stresses are larger in the rise direction than in the plane normal to it; this is a common observation [13, 14, 16–19].

0022–2461/88 $03.00 + .12

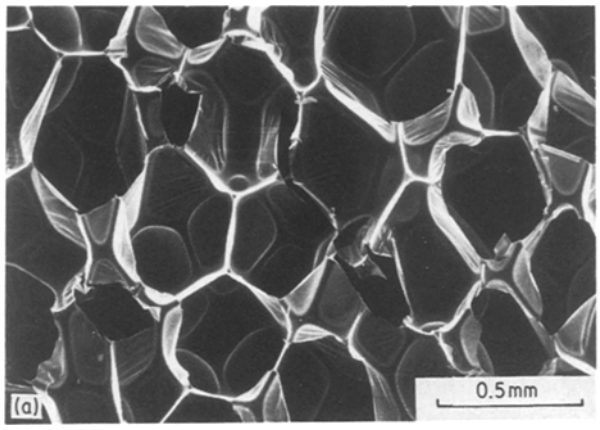

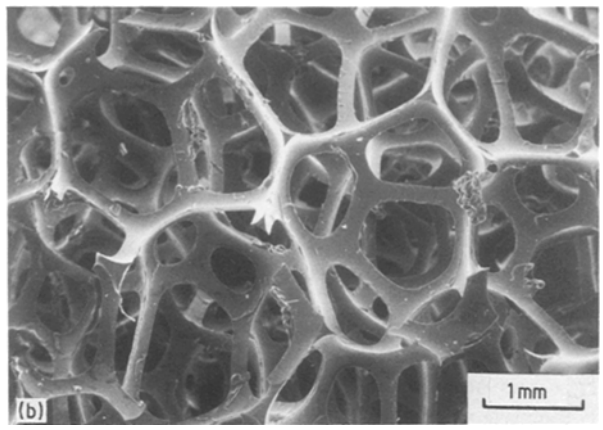

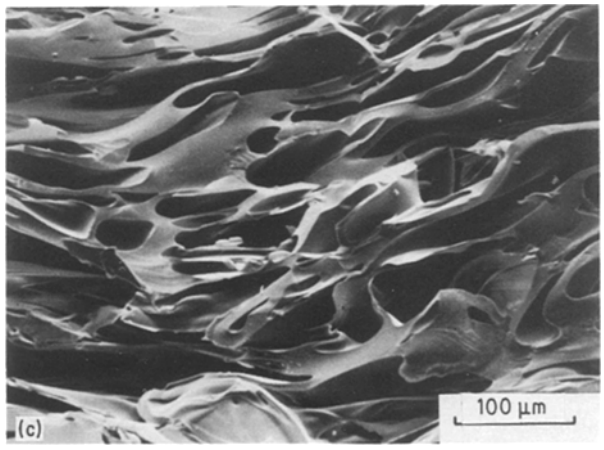

Figure 1 Scanning electron micrographs of (a) an axisymmetric rigid polyurethane foam with a shape-anisotropy ratio, R of 1.4 ($\varrho = 32\,\mathrm{kg\,m^{-3}}$), (b) an axisymmetric elastomeric polyurethane foam with a shape-anisotropy ratio, R of 1.2 ($\varrho = 28\,\mathrm{kg\,m^{-3}}$), and (c) pumice, a natural foam. Deformation of the pumice while still viscous has distorted the cells giving a shape-anisotropy ratio, R, of 6.

Here, for simplicity, we analyse anisotropy in axisymmetric open-cell foam structures. The cell wall material is assumed to be isotropic so that the anisotropy of the foam arises solely from cell shape. In practice, the cell wall material may, itself, be anisotropic, as it is in wood, for instance: this then gives an additional contribution to anisotropy. Closed-cell foams tend to behave like open-cell ones if, as is often the case, the membranes across the cell faces are thin relative to the cell edges. The method is easily generalized to foams with orthotropic symmetry; the results are given in the Appendix. It is a simple extension of the model developed by Gibson and Ashby [4] and Maiti *et al.* [8]. It differs fundamentally from those adapted by Kanakkanatt [13], Mehta and Colombo [14], Cunningham [15] and Hilyard [16] who implicitly assume that all foam properties depend linearly on relative density.

3.1. Linear elasticity: the moduli

Fig. 3 shows an idealized open cell, typifying that in an

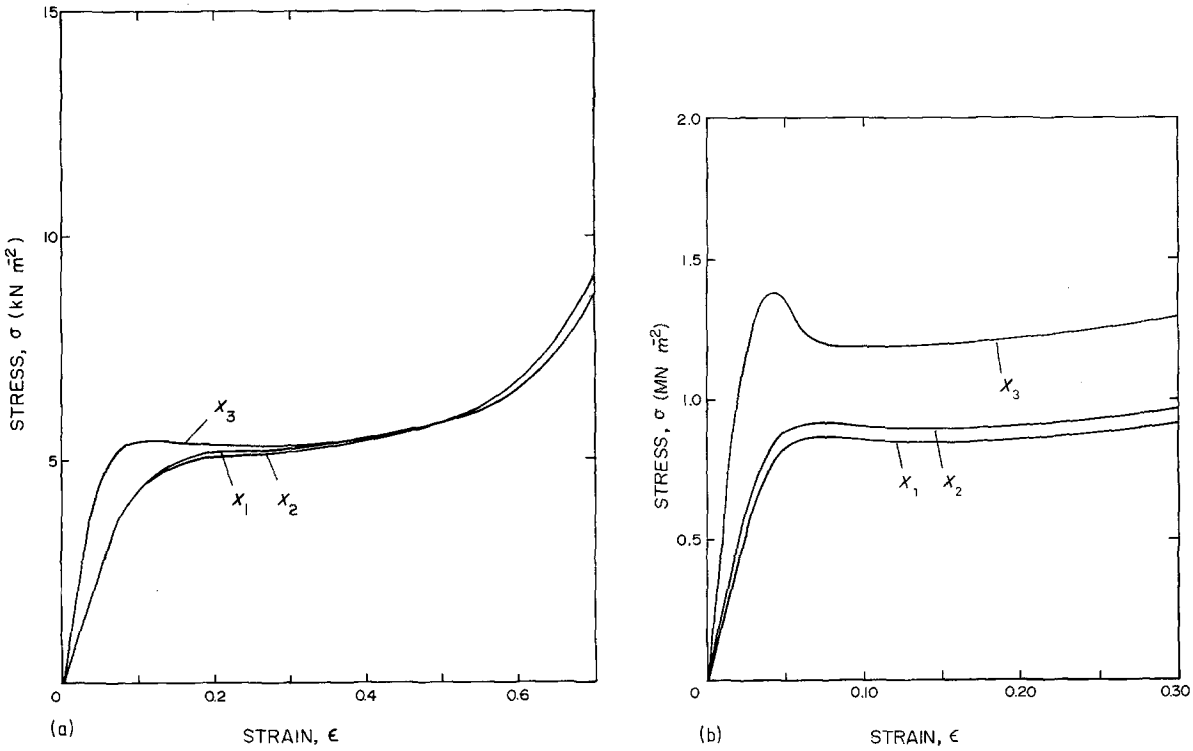

Figure 2 Typical compressive stress–strain curves for loading in two orthogonal directions in the plane normal to the rise direction (X_1 and X_2) and in the rise direction (X_3) for (a) a flexible polyurethane foam ($\varrho = 28\,\mathrm{kg\,m^{-3}}$, 0.62 mm nominal cell size) and (b) a rigid polyurethane foam ($\varrho = 96\,\mathrm{kg\,m^{-3}}$).

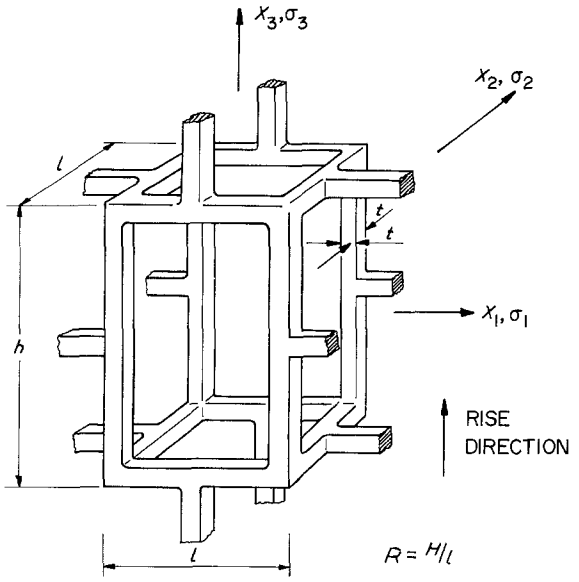

Figure 3 An axisymmetric unit cell with a shape-anisotropy ratio, R of 1.5.

axisymmetric foam: the rise direction is parallel to X_3. Let the Young's modulus of the foam in the rise direction be E_3^*, and that in the two directions normal to this be $E_1^* = E_2^*$. We seek to calculate the ratio E_3^*/E_1^* in terms of the anisotropy ratio, $R = h/l$.

A load in the X_3 direction is carried by the four beams of length l, which respond by bending (Fig. 4a). The force, F, on each beam is proportional to $\sigma_3 l^2$, and the deflection, δ_3, of each is proportional to $Fl^3/E_s I$ (where E_s is the modulus of the solid and I the second moment of area of the cell edge). The strain ε_3 is related to the displacement δ_3 by $\varepsilon_3 \propto \delta_3/h$, where h is the height of the cell. Assembling these, we find

$$\begin{aligned} E_3^* &= \frac{\sigma_3}{\varepsilon_3} \\ &= \frac{CE_s Ih}{l^5} \\ &= CE_s\left(\frac{t}{l}\right)^4 \frac{h}{l} \end{aligned}$$

where C is a constant of proportionality. The equation reduces to the result for an isotropic foam given by Gibson and Ashby [4] when $h = l$, as, of course, it should.

A load in the X_1 direction is carried by two beams of length l and two of length h (Fig. 4b). The deflection, δ_1, of both sets must be equal, so that the load carried by the longer beams is less than that carried by the shorter ones; the first is proportional to $E_s I/h^3$, the other to $E_s I/l^3$. The total force is proportional to $\sigma_1 hl$, and the strain, ε_1, to δ_1/l. Assembling these, we obtain

$$\begin{aligned} E_1^* &= \frac{\sigma_1}{\varepsilon_1} = \frac{CE_s I}{2h}\left(\frac{1}{l^3} + \frac{1}{h^3}\right) \\ &= \frac{CE_s}{2}\left(\frac{t}{l}\right)^4 \left(\frac{l}{h}\right)\left[1 + \left(\frac{l}{h}\right)^3\right] \end{aligned}$$

which, again, reduces to the isotropic result when $h = l$. Taking the ratio of these two equations, and writing $R = h/l$ gives the Young's modulus anisotropy ratio

$$\frac{E_3^*}{E_1^*} = \frac{2R^2}{1 + (1/R^3)} \qquad (1)$$

Because loading in the rise direction deflects the shorter cell edges, of length l, the stiffness in the rise direction is greater than that for loading in the plane normal to it. The modulus ratio depends strongly on anisotropy: cells with a shape anisotropy of 2 have a modulus anisotropy of nearly 8.

A similar analysis for the shear modulus shows that it is much less sensitive to anisotropy in cell shape. For loading in the X_1–X_2 plane (Fig. 5a), we find that the load acting on each member of length l is proportional to $\tau_{12} hl$ and that the deflection of each member of length l is proportional to $\tau_{12} hl^4/E_s t^4$. The shear strain, γ_{12}, is proportional to δ/l giving a shear modulus in the X_1–X_2 plane of

$$\begin{aligned} G_{12}^* &= \frac{\tau_{12}}{\gamma_{12}} \\ &= CE_s\left(\frac{t}{l}\right)^4 \left(\frac{l}{h}\right) \end{aligned}$$

where C is again a constant of proportionality. For loading in the X_1–X_3 plane, the load is shared between two members of length l and two of length h (Fig. 5b). Equilibrium requires that $P_3 = P_1 h/l$ (P_1 and P_3 are loads acting in the X_1 and the X_3 directions, respectively). The deflections of the beams of length h and l are proportional to $P_1 h^3/E_s t^4$ and $P_3 l^3/E_s t^4$ respectively, giving a shear strain of $\gamma = \gamma_1 + \gamma_3 \propto \delta_1/h +$

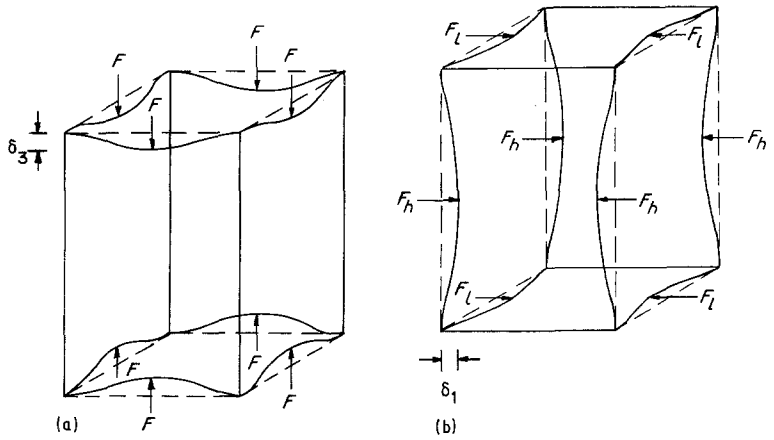

Figure 4 Linear elastic deformation of the axisymmetric cell under uniaxial loading in (a) the X_3 direction and (b) the X_1 or X_2 direction.

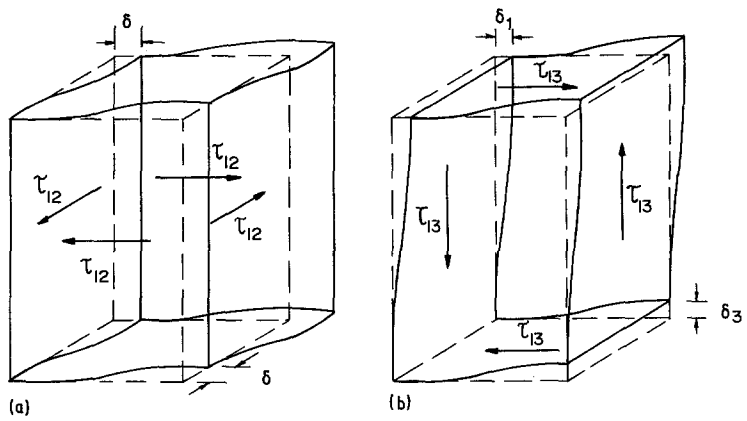

Figure 5 Shear deformation of the axisymmetric cell in (a) the X_1–X_2 plane and (b) the X_1–X_3 plane.

$\delta_3/l \propto P_1(h^2 + hl)/E_s t^4$. The resulting shear modulus in the X_1–X_3 plane is

$$G^*_{13} = 2CE_s\left(\frac{t}{l}\right)^4\left(\frac{l}{h}\right)\frac{1}{(h/l) + 1}$$

and the shear modulus anisotropy ratio is

$$\frac{G^*_{13}}{G^*_{12}} = \frac{2}{1 + R} \tag{2}$$

Poisson's ratio is the negative ratio of a lateral to an applied strain. As a result, it is independent of relative density and depends only on the cell geometry. Dimensional arguments of the type used to calculate the Young's modulus and the shear modulus offer no insight into its dependence on cell geometry. We do not attempt a calculation of it here.

3.2. Non-linear elasticity: the elastic collapse stress

For loading in the X_3 direction (Fig. 6), cell walls buckle when the load on them exceeds the Euler load, $F_{cr} = n_3^2\pi^2 E_s I/h^2$ where n_3 describes the rotational stiffness at the ends of the column for this direction of loading; it is related to the flexural stiffness of the members of length l. The load, F, is proportional to $\sigma_3 l^2$ giving

$$(\sigma^*_{el})_3 = \frac{Cn_3^2\pi^2 E_s I}{h^2 l^2}$$

where C is again a constant of proportionality.

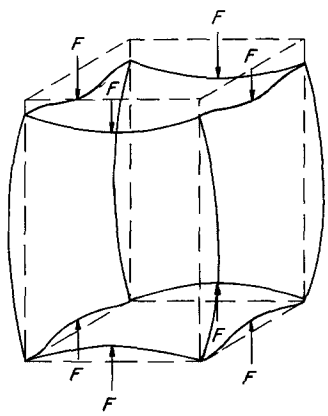

Figure 6 Elastic buckling of the axisymmetric cell under uniaxial loading in the X_3 direction.

Similarly, for loading in the X_1 direction, $F_{cr} = n_1^2\pi^2 E_s I/l^2$ and $F \propto \sigma_1 hl$ giving:

$$(\sigma^*_{el})_1 = \frac{Cn_1^2\pi^2 E_s I}{hl^3}$$

In this case, n_1 is the rotational stiffness at the ends of the column for loading in the X_1 direction and depends on the flexural stiffness of both the members of length l and of length h. Taking the ratio of these two and inserting $R = h/l$ gives the elastic collapse ratio

$$\frac{(\sigma^*_{el})_3}{(\sigma^*_{el})_1} = \frac{n_3^2}{n_1^2}\frac{1}{R} \tag{3}$$

At first sight it appears that loading in the rise direction, X_3, should produce buckling at a lower load (and a lower elastic collapse stress) than for loading in either the X_1 or the X_2 direction. But there is an additional effect controlling buckling. The rotational constraint at the ends of the long columns, n_3, is greater than that at the shorter ones, n_1, tending to stabilize them. Experiments, described below, show that these two competing effects almost cancel, giving a weak dependence on R.

3.3. Plastic collapse

Plastic collapse occurs when two plastic hinges form in each cell edge; this requires that the fully plastic moment, M_p, of the cell wall is exceeded. For loading in the X_3 direction (Fig. 4a), four edges of length l must collapse. The moment, M_p, on each is proportional to Fl and the force, F, is proportional to $\sigma_3 l^2$, giving

$$(\sigma^*_{pl})_3 = \frac{CM_p}{l^3}$$

where C, once again, is a constant of proportionality. For loading in the X_1 direction, on the other hand, two edges of length l and two of length h must collapse (Fig. 4b). The first pair support a force proportional to M_p/l, while the other pair support a force proportional to M_p/h. The total force is $\sigma_1 lh$, giving

$$(\sigma^*_{pl})_1 = \frac{CM_p}{2lh}\left(\frac{1}{l} + \frac{1}{h}\right)$$

Taking the ratio and substituting $R = h/l$ leads to the plastic collapse ratio

$$\frac{(\sigma^*_{pl})_3}{(\sigma^*_{pl})_1} = \frac{2R}{1 + (1/R)} \tag{4}$$

The cells are thus stronger in the rise direction, although the anisotropy in strength is not as large as that in stiffness (Equation 1): cells with a shape anisotropy of 2 should have a plastic strength anisotropy of around 2.6.

3.4. Brittle crushing

The argument for the crushing strength, σ^*_{cr}, parallels that for plastic collapse with the yield strength of the cell wall replaced by its modulus of rupture. The result in Equation 4 with σ^*_{pl} replaced by σ^*_{cr}.

3.5. The fracture toughness

The fracture toughness of an anisotropic foam depends on the direction in which the crack propagates. This is best defined with two subscripts, the first indicating the normal to the crack plane, the second the direction of crack propagation: thus $(K^*_{fc})_{31}$ is the fracture toughness associated with a crack on the plane normal to X_3, advancing in the X_1 direction; the crack front lies parallel to X_2.

A far-away tensile stress applied in the X_3 direction, σ_3^∞, produces a local stress at a distance r ahead of the crack tip of (Fig. 7)

$$(\sigma_3)_{local} = \frac{\sigma_3^\infty (\pi a)^{1/2}}{(2\pi r)^{1/2}} = \frac{(K^*_{fc})_{31}}{(2\pi r)^{1/2}}$$

for a crack of length $2a$. The distance ahead of the crack tip to the next cell wall to fracture is proportional to l. The force acting on the next cell wall is proportional to $(\sigma_3)_{local} l^2$ while the moment is proportional to that force times the length l

$$M = (\sigma_3)_{local} l^3$$

Cell wall fracture occurs when the stress in the member reaches the modulus of rupture of the solid, σ_{fs}, or when the applied moment is proportional to $\sigma_{fs} t^3$. Combining these expressions we obtain

$$(\sigma_3)_{local} = C\sigma_{fs}\left(\frac{t}{l}\right)^3 = \frac{C\sigma_3^\infty (\pi a)^{1/2}}{(\pi l)^{1/2}} = \frac{C(K^*_{fc})_{31}}{(\pi l)^{1/2}}$$

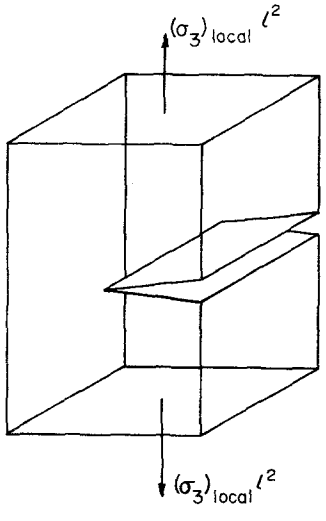

Figure 7 Crack propagation in the axisymmetric cell for $(K^*_{fc})_{31}$.

TABLE I Anisotropy in axisymmetric foams

$\frac{E_3^*}{E_1^*} = \frac{2R^2}{1 + (1/R^3)}$	$(E_1^* = E_2^*)$
$\frac{G_{13}^*}{G_{12}^*} = \frac{2}{1 + R}$	$(G_{13}^* = G_{23}^*)$
$\frac{(\sigma_{el}^*)_3}{(\sigma_{el}^*)_1} = \frac{n_3^2}{n_1^2}\frac{1}{R}$	$(\sigma_{el}^*)_1 = (\sigma_{el}^*)_2$
$\frac{(\sigma_{pl}^*)_3}{(\sigma_{pl}^*)_1} = \frac{2R}{1 + (1/R)}$	$(\sigma_{pl}^*)_1 = (\sigma_{pl}^*)_2$
$\frac{(\sigma_{cr}^*)_3}{(\sigma_{cr}^*)_1} = \frac{2R}{1 + (1/R)}$	$(\sigma_{cr}^*)_1 = (\sigma_{cr}^*)_2$
$\frac{(K^*_{fc})_{31}}{(K^*_{fc})_{12}} = R$	$(K^*_{fc})_{31} = (K^*_{fc})_{32}$
$\frac{(K^*_{fc})_{31}}{(K^*_{fc})_{13}} = R^{3/2}$	$(K^*_{fc})_{13} = (K^*_{fc})_{23}$
$\frac{(K^*_{fc})_{12}}{(K^*_{fc})_{13}} = R^{1/2}$	$(K^*_{fc})_{12} = (K^*_{fc})_{21}$

or

$$(K^*_{fc})_{31} = C\sigma_{fs}\left(\frac{t}{l}\right)^3 (\pi l)^{1/2}$$

Similarly, we obtain for $(K^*_{fc})_{12}$ and $(K^*_{fc})_{13}$

$$(K^*_{fc})_{12} = C\sigma_{fs}\left(\frac{t}{l}\right)^3 \frac{l}{h} l^{1/2}$$

$$(K^*_{fc})_{13} = C\sigma_{fs}\left(\frac{t}{l}\right)^3 \left(\frac{l}{h}\right)^2 h^{1/2}$$

Note that by symmetry, $(K^*_{fc})_{32} = (K^*_{fc})_{31}$, $(K^*_{fc})_{21} = (K^*_{fc})_{12}$, and $(K^*_{fc})_{23} = (K^*_{fc})_{13}$. The ratios of the fracture toughness for a given crack length, a, are

$$\frac{(K^*_{fc})_{31}}{(K^*_{fc})_{12}} = R \quad (5a)$$

$$\frac{(K^*_{fc})_{31}}{(K^*_{fc})_{13}} = R^{3/2} \quad (5b)$$

$$\frac{(K^*_{fc})_{12}}{(K^*_{fc})_{13}} = R^{1/2} \quad (5c)$$

The sensitivity of the fracture toughness to anisotropy depends on the direction of loading and on the direction of crack propagation. A shape-anisotropy ratio of 2 produces a fracture toughness ratio of between 1.4 and 2.8.

The results of the analysis for axisymmetric foams are summarized in Table I. The method can easily be extended to the orthotropic case; the results are given in the Appendix.

4. Experimental methods

The principal mean intercept lengths and mechanical properties of flexible and rigid polyurethane foams were measured. The flexible foam specimens all had a nominal density of $28\,kg\,m^{-3}$ and mean cell sizes of 0.33, 0.43, 0.62, 0.82 and 1.95 mm. The rigid foam specimens had nominal densities of 32, 64, 96, 128, and $160\,kg\,m^{-3}$. Cubic specimens of both types of foam were cut with one pair of faces normal to the rise direction indicated by the manufacturer.

The mean intercept lengths of the foam specimens

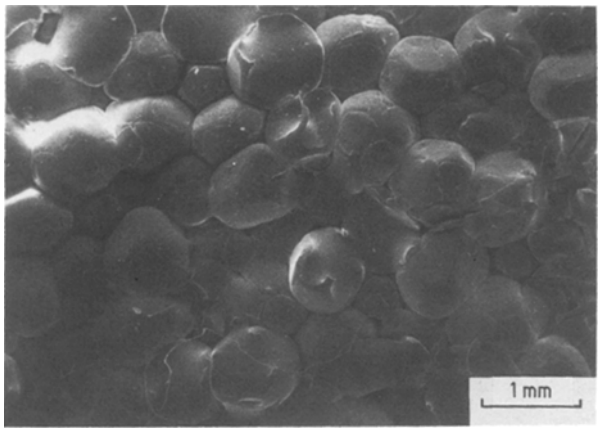

Figure 8 A micrograph of a replica of the flexible polyurethane foam (ϱ = 28 kg m^{-3}; nominal cell size = 0.43 mm).

were measured using digital image analysis of low magnification scanning electron micrographs. For the microscopy, small cubes of foam (about 5 mm on a side) were cut from a large block, adjacent to the area from which the mechanical test specimens were taken. The specimens were gold-coated and viewed in the SEM at 0° tilt to eliminate distortion. On the micrographs of the open-cell foams it was difficult to identify a single layer of cells; to overcome this difficulty replicas of each surface of these foams were made using Xantropren blue, a silicon-based plastic. The replicas were then photographed in the SEM; a typical example is shown in Fig. 8. Two specimens of each of the three perpendicular faces of each density of the rigid foam and of each cell size of the flexible foam were viewed. At least three micrographs of different locations on each specimen were taken.

The micrographs of the foam structure were digitized using a bit pad and a digitizing pen. The mean intercept length of the cells was then calculated from the digitized micrograph using a computer program to count the number of intercepts along test lines at 10° intervals through a full 180° rotation. For each angle of rotation, between 5 and 50 test lines were analysed. The data for the intercept length as a function of angle of rotation was then fitted to an ellipse using a least squares routine. The eccentricity of the ellipse gave the ratio of the principal mean cell lengths in the plane of the micrograph. A typical micrograph, digitized picture and best-fit ellipse for a rigid polyurethane foam are shown in Fig. 9. This procedure was repeated for micrographs in three orthogonal planes for each specimen.

The mechanical properties of the foams were measured for loading in the rise direction and for loading in two orthogonal directions normal to the rise direction. 50 mm cubes of both the rigid and the flexible foam were loaded in compression in an Instron testing machine which recorded the load and deflection during the test. Young's moduli and the elastic or plastic collapse stresses were calculated from the load–deflection curves. The fracture toughness of the rigid foam was measured on 25 mm × 25 mm × 375 mm notched beams (notch length = 12.5 mm) loaded in three-point bending.

5. Results

The results of the tests are summarized in Tables II to IV. Table II shows the ratios of the mean intercept lengths of the cells. Three ratios are calculated from the measurements; the consistency of these results can be observed by comparing the value of R_{32} calculated

TABLE II Measured shape-anisotropy ratios. Foam rise is in the X_3 direction. Standard deviations are given below each mean

Foam type	Nominal cell size (mm)	Density (kg m^{-3})	$R^*_{21} = l_2/l_1$	$R_{32} = l_3/l_2$	$R_{31} = l_3/l_1$	A† or O	$R_{32} = R_{31}/R_{21}$	$R = \frac{R_{32} + R_{31}}{2}$
Flexible polyurethane (ϱ = 28 kg m^{-3})	0.33		1.13	1.15	1.18	A	1.04	1.17
			0.06	0.03	0.11			
	0.43		0.88	1.20	1.17	A	1.33	1.19
			0.07	0.05	0.09			
	0.62		1.04	1.26	1.31	A	1.26	1.29
			0.04	0.04	0.04			
	0.82§		0.91	1.26	1.21	A	1.33	1.24
			0.02	0.12	0.13			
	1.95		0.91	1.26	1.25	A	1.38	1.26
			0.10	0.11	0.04			
Rigid polyurethane		32	0.88	1.48	1.33	A	1.50	1.41
			0.08	0.09	0.11			
		64	1.12	1.39	1.55	A	1.38	1.47
			0.06	0.12	0.18			
		96	0.87	1.30	1.16	A	1.33	1.23
			0.07	0.15	0.01			
		128‡	1.13	1.13	1.42	O	1.26	1.28
			0.03	–	0.04			
		160§	1.10	1.19	1.19	A	1.08	1.19
			0.01	0.08	0.06			

*l_i is the mean intercept length of the foam in the X_i direction and $R_{ij} = l_i/l_j$.
†A = axisymmetric (R_{12} = 1.0 and $R_{32} = R_{31}$); O = orthotropic ($R_{12} \neq R_{32} \neq R_{31}$).
‡Only one measurement for R_{32} was made for this foam due to difficulties with the microscopy. It was taken to be orthotropic because R_{21} differs significantly from 1.0 and E_1 differs significantly from E_2.
§For these two foams R_{12} differs significantly from 1.0 due to the low sample standard deviations. R_{32} does not vary significantly from R_{31} however; because of this both foams were taken to be axisymmetric.

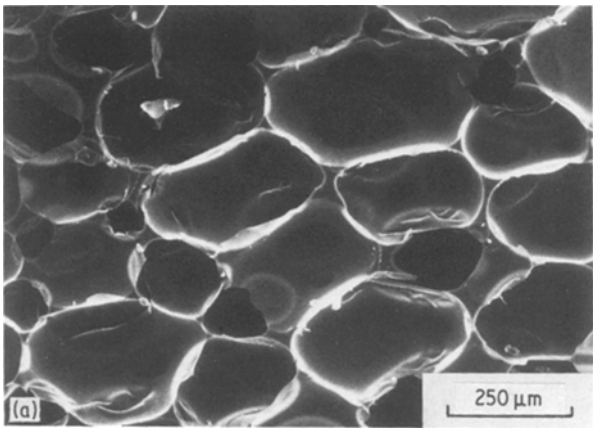

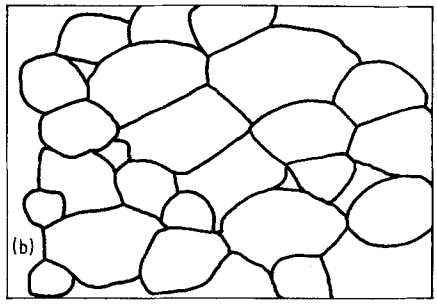

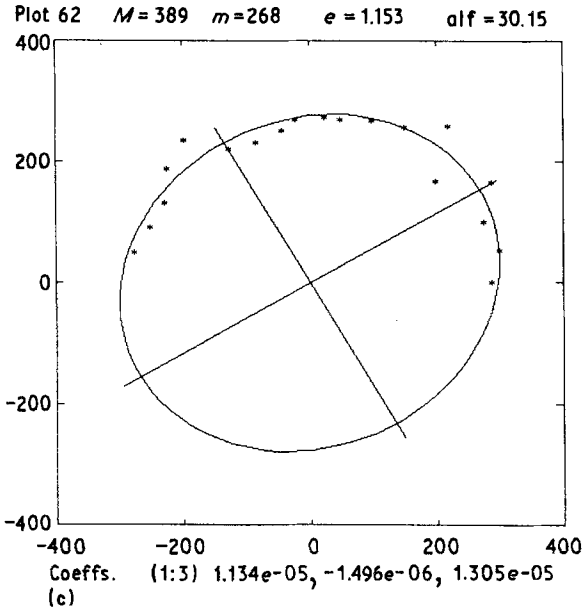

Figure 9 The measurement of the shape-anisotropy ratio, R. (a) A micrograph of a rigid polyurethane foam ($\varrho = 96\,\mathrm{kg\,m^{-3}}$), (b) the digitized micrograph, and (c) the best-fit ellipse calculated from the mean intercept lengths of test lines at 10° intervals.

from the ratio of l_3/l_2 and that found by taking the ratio of R_{31}/R_{21}. The results are encouraging; in all cases the two values are within 10% of each other. A t-test with 95% confidence intervals indicated that there was no significant difference between the X_1 and X_2 directions for all of the foams except the $128\,\mathrm{kg\,m^{-3}}$ rigid polyurethane. With this one exception, the foams are axisymmetric and are described by a single shape-anisotropy ratio, $R = h/l$. The variation in R with cell size and density is shown in Fig. 10.

Typical compressive stress–strain curves for the flexible and rigid polyurethane foams were shown in Fig. 2. Young's modulus was calculated from the initial slope of the curve. The elastic collapse stress of the flexible foam was taken to be the stress at which the two straight lines of the linear elastic portion and the plateau portion intersect. The plastic collapse stress of the rigid polyurethane foam was taken to be the upper yield stress before the stress plateau. The load–deflection curves for the fracture toughness tests on the rigid foams were all linear elastic up to the point of fracture. The results of the mechanical tests are summarized in Tables III and IV for the flexible and rigid foams, respectively. As with the data for the mean intercept lengths, the mechanical properties of the foams indicate that they are roughly axisymmetric: the data can then be plotted in terms of a property ratio (the property in the X_3 direction to the average of the property in the X_1 and the X_2 directions) as a function of a single shape-anisotropy ratio, $R = (R_{32} + R_{31})/2$. Data for the Young's modulus, the elastic and plastic collapse stresses and the fracture toughness of axisymmetric foams with shape-anisotropy ratios varying from 1 to 1.6 are shown in Figs 11 to 14. The data for the $128\,\mathrm{kg\,m^{-3}}$ rigid polyurethane foam has been omitted from the plots as it is orthotropic rather than axisymmetric; the equations for orthotropic foams given in the Appendix describe these results reasonably well. The data for the 1.95 mm flexible polyurethane has also been omitted as it is far out of line with the rest of the data. The

TABLE III Experimental results for Young's modulus and the elastic collapse stress for flexible polyurethane foams. Foam rise in the X_3 direction. The standard deviation for each property is given below the mean value

Nominal cell size (mm)	Young's modulus ($\mathrm{kN\,m^{-2}}$)			Elastic collapse stress ($\mathrm{kN\,m^{-2}}$)		
	E_1^*	E_2^*	E_3^*	$(\sigma_{el})_1^*$	$(\sigma_{el})_2^*$	$(\sigma_{el})_3^*$
0.33	145	161	273	5.57	5.79	6.09
	8.6	9.4	22	0.13	0.17	0.18
0.43	101	138	206	4.76	5.62	5.41
	3.7	6.9	16	0.07	0.14	0.18
0.62	108	109	213	4.93	4.88	5.43
	1.8	4.0	7.5	0.06	0.26	0.08
0.82	97.7	107	213	4.83	4.99	5.47
	6.6	3.7	14	0.10	0.13	0.10
1.95	62.8	65.8	275	3.39	3.43	5.30
	3.7	4.2	20	0.16	0.19	0.06

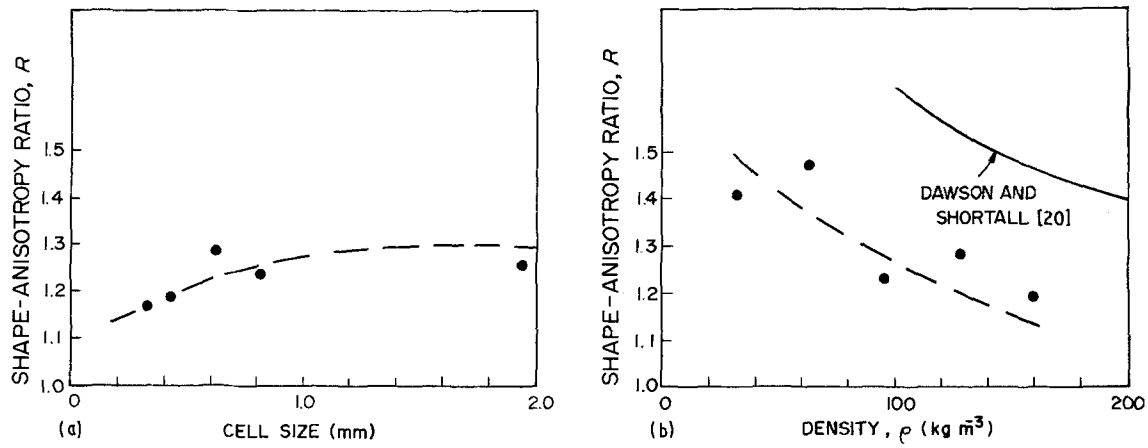

Figure 10 The shape-anisotropy ratio, R, plotted against (a) cell size and (b) density. (a) Flexible polyurethane foam, nominal density 28 kg m^{-3}; (b) rigid polyurethane foam, nominal cell size 0.2 mm.

reason for this is not clear; it may be that the measured shape-anisotropy ratios are less reliable for this foam as fewer cells were measured or it may be that there is a size effect which had not been modelled.

6. Discussion

All of the foams, with the exception of the 128 kg m^{-3} rigid polyurethane, are axisymmetric with a shape-anisotropy ratio, R, of between 1.1 and 1.5. The shape-anisotropy ratio tends to increase with cell size and decrease with density. Dawson and Shortall [20] found a similar dependence on density, although shifted relative to the data reported here (Fig. 10). This effect is expected intuitively. As the thickness of the cell wall increases with density (for cells of the same size), the interal gas pressure within the cell cannot lift the additional weight of the cell wall as high, reducing the elongation of the cell.

As expected, Young's modulus is the most sensitive property to anisotropy in the shape of the cells, with ratios of E_3^*/E_1^* of up to 4 measured. The solid line of Fig. 11, given by Equation 1, describes the data of this study and several others well. The next most sensitive property to anisotropy in cell shape is the plastic collapse stress, and it, too, is well described by the model (Equation 4, solid line in Fig. 13) with only a slight underprediction of the data.

The results for the remaining two properties, the elastic collapse stress and the fracture toughness, are more difficult to interpret. Both are much less sensitive to anisotropy in cell shape. As indicated in the analysis, there appear to be two competing effects determining the elastic buckling load: the length of the column and the end rotational stiffness. The first leads to a lower buckling stress in the rise direction (so that the ratio $(\sigma_{el}^*)_3/(\sigma_{el}^*)_1$ is less than 1); the second clearly increases the buckling stress in the rise direction, but it is difficult to estimate by how much. The data indicate a weak dependence on the shape-anisotropy ratio of roughly $R^{1/2}$ (dashed line, Fig. 12).

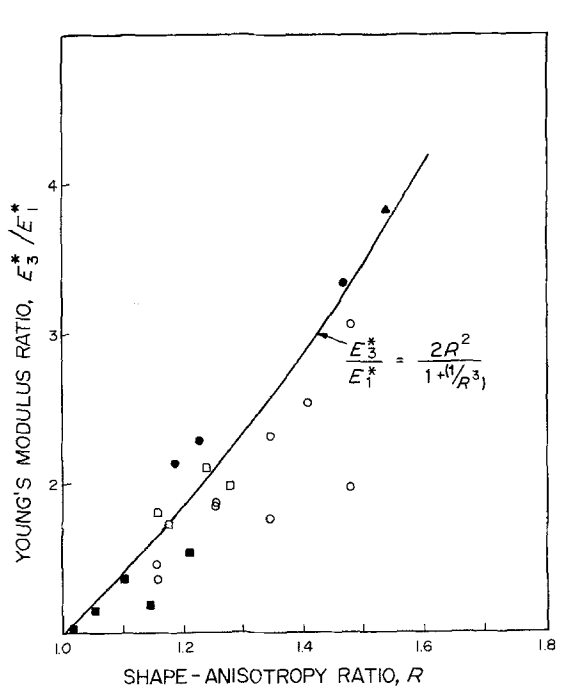

Figure 11 The Young's modulus ratio E_3^*/E_1^*, plotted against the shape-anisotropy ratio, R. The solid line is given by Equation 1. (●) PU(R), (□) PU(F), both present work; (▲) polyisocyanurate, Gupta *et al.* [19]; (○) PU(F), Hilyard [16]; (■) PS, Metha and Colombo [14].

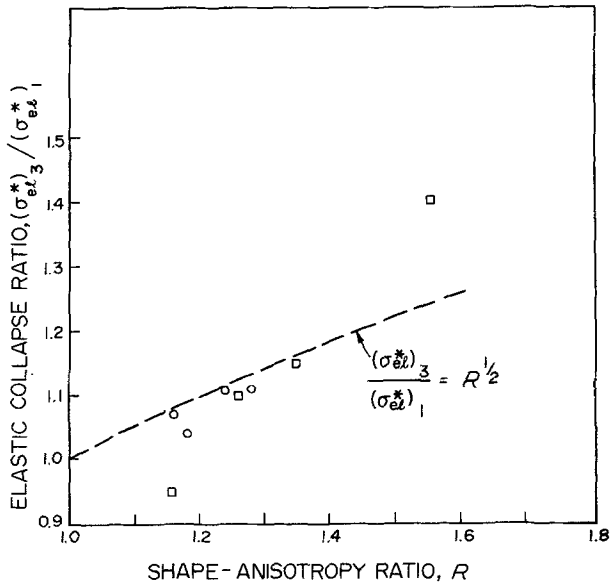

Figure 12 The elastic collapse stress ratio, $(\sigma_{el}^*)_3/(\sigma_{el}^*)_1$, plotted against the shape-anisotropy ratio, R. (○) PU(F), present work, (□) PU(F), Hilyard [16].

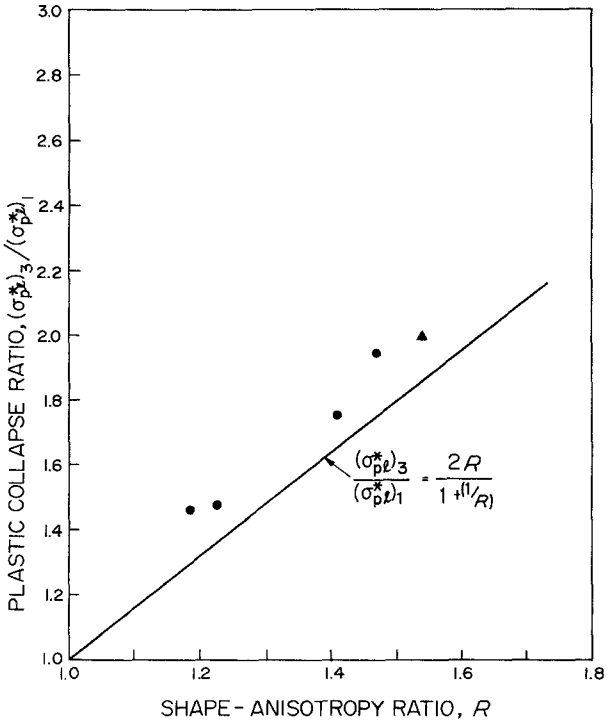

Figure 13 The plastic collapse stress ratio, $(\sigma^*_{pl})_3/(\sigma^*_{pl})_1$, plotted against the shape-anisotropy ratio, R. The solid line is given by Equation 4. (●) PU(R), present work; (▲) polyisocyanurate, Gupta *et al.* [19].

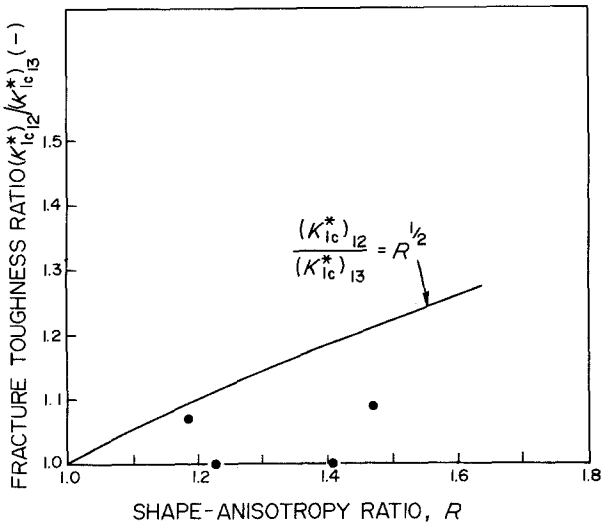

Figure 14 The fracture toughness ratio, $(K^*_{Ic})_{12}/(K^*_{Ic})_{13}$, plotted against the shape-anisotropy ratio, R. The solid line is given by Equation 5. (●) PU(R), present work.

Because of limitations in the available dimensions of specimens for the fracture toughness tests, the fracture toughness ratio was measured only in the direction we expect to be the least sensitive ($(K^*_{Ic})_{12}/(K^*_{Ic})_{13} = R^{1/2}$). The data show even less dependence on cell shape than this; for values of R up to 1.5, there is virtually no dependence of $(K^*_{Ic})_{12}/(K^*_{Ic})_{13}$ on cell shape. Additional tests for the fracture toughness ratios are required to understand the effect of anisotropy more fully.

7. Conclusions

The model of Gibson and Ashby [4] has been extended to describe anisotropy in foams. Equations for the ratios of the moduli, the elastic, plastic and brittle collapse stresses and of the fracture toughnesses in the rise direction to those in the plane normal to it are given. Measurements of cell shape and mechanical properties for a flexible and a rigid polyurethane foam indicate that the equations for the Young's modulus ratio and the plastic collapse ratio, the two most sensitive properties to cell shape, describe the data well. Additional modelling of the effect of the column end restraint is needed to understand the effect of cell shape on the elastic collapse stress ratio. Additional data for the fracture toughness of foams loaded in all three directions and with all possible crack propagation orientations are also necessary to understand further anisotropy in foams.

Acknowledgements

We are grateful to Professor M. F. Ashby, Cambridge University Engineering Department, UK, for helpful discussions on the modelling of anisotropy and to Professor L. N. Trefethen, Department of Mathematics, Massachusetts Institute of Technology, for the provision of the ellipse fitting program for the mean intercept length data. We would also like to thank Mr Len Sudenfield, Center for Materials Science and Engineering, Massachusetts Institute of Technology, for his technical assistance with the scanning electron microscopy. Foam specimens were given by Scotfoam of Eddystone, Pennsylvania, and General Plastics of Tacoma, Washington. Financial support for this project was provided by the Solid

TABLE IV Experimental results for Young's modulus, the plastic collapse stress and fracture toughness for rigid polyurethane foams. Foam rise in the X_3 direction. The standard deviation for each property is given below the mean value

Density ($kg\,m^{-3}$)	Young's modulus ($MN\,m^{-2}$)			Plastic collapse stress ($MN\,m^{-2}$)			Fracture toughness ($kN\,m^{-3/2}$)	
	E_1^*	E_2^*	E_3^*	$(\sigma^*_{pl})_1$	$(\sigma^*_{pl})_2$	$(\sigma^*_{pl})_3$	$(K^*_{Ic})_{12}$	$(K^*_{Ic})_{13}$
32	1.23	1.28	3.16	0.121	0.123	0.211	16.7	16.3
	0.07	0.13	0.30	0.002	0.009	0.006	0.9	0.9
64	3.41	4.50	13.1	0.329	0.373	0.682	35.4	38.0
	0.50	0.77	2.37	0.019	0.041	0.068	0.9	1.1
96	11.3	11.4	25.6	0.862	0.876	1.290	61.5	62.0
	0.77	1.54	2.66	0.038	0.067	0.022	1.6	2.5
128	19.3	21.8	30.3	1.41	1.56	1.71	60.9	64.8
	1.21	1.72	1.90	0.040	0.038	0.018	2.3	0.9
160	21.7	24.1	48.6	1.70	1.86	2.59	128	137
	0.45	0.90	1.74	0.041	0.110	0.095	6.4	11

Mechanics Program of the National Science Foundation, Grant no. MSM 8603821, which we greatly appreciate.

Appendix. Summary of equations for orthotropic cellular solids

Property	Orthotropic case
$\frac{E_1^*}{E_2^*}$	$(R_{12})^2\left[\frac{1+(R_{32})^3}{1+(R_{31})^3}\right]$
$\frac{E_2^*}{E_3^*}$	$(R_{23})^2\left[\frac{1+(R_{13})^3}{1+(R_{12})^3}\right]$
$\frac{E_3^*}{E_1^*}$	$(R_{31})^2\left[\frac{1+(R_{21})^3}{1+(R_{23})^3}\right]$
$\frac{G_{12}^*}{G_{23}^*}$	$\frac{1+R_{32}}{1+R_{12}}$
$\frac{G_{23}^*}{G_{31}^*}$	$\frac{1+R_{13}}{1+R_{23}}$
$\frac{G_{31}^*}{G_{12}^*}$	$\frac{1+R_{21}}{1+R_{31}}$
$\frac{(\sigma_1)_{el}^*}{(\sigma_2)_{el}^*}$	R_{21}
$\frac{(\sigma_2)_{el}^*}{(\sigma_3)_{el}^*}$	R_{32}
$\frac{(\sigma_3)_{el}^*}{(\sigma_1)_{el}^*}$	R_{13}
$\frac{(\sigma_1)_{pl}^*}{(\sigma_2)_{pl}^*}$	$(R_{12})^2\left[\frac{1+(R_{23})}{1+(R_{13})}\right]$
$\frac{(\sigma_2)_{pl}^*}{(\sigma_3)_{pl}^*}$	$(R_{23})^2\left[\frac{1+(R_{31})}{1+(R_{21})}\right]$
$\frac{(\sigma_3)_{pl}^*}{(\sigma_1)_{pl}^*}$	$(R_{31})^2\left[\frac{1+(R_{12})}{1+(R_{32})}\right]$
$\frac{(\sigma_1)_{cr}^*}{(\sigma_2)_{cr}^*}$	$(R_{12})^2\left[\frac{1+(R_{23})}{1+(R_{13})}\right]$
$\frac{(\sigma_2)_{cr}^*}{(\sigma_3)_{cr}^*}$	$(R_{23})^2\left[\frac{1+(R_{31})}{1+(R_{21})}\right]$
$\frac{(\sigma_3)_{cr}^*}{(\sigma_1)_{cr}^*}$	$(R_{31})^2\left[\frac{1+(R_{12})}{1+(R_{32})}\right]$
$\frac{(K_{Ic})_{ik}^*}{(K_{Ic})_{jk}^*}$	R_{ij}
$\frac{(K_{Ic})_{ij}^*}{(K_{Ic})_{ji}^*}$	$(R_{ij})^{3/2}$
$\frac{(K_{Ic})_{ki}^*}{(K_{Ic})_{kj}^*}$	$(R_{ji})^{1/2}$
$\frac{(K_{Ic})_{ki}^*}{(K_{Ic})_{jk}^*}$	$R_{kj}(R_{ki})^{1/2}$
$\frac{(K_{Ic})_{ik}^*}{(K_{Ic})_{kj}^*}$	$R_{ik}(R_{jk})^{1/2}$

l_i is the mean intercept length of the foam in the X_i direction and $R_{ij} = l_i/l_j$.

References

1. W. L. KO, *J. Cell. Plast.* **1** (1965) 45.
2. M. R. PATEL and I. FINNIE, *J. Mater.* **5** (1970) 909.
3. G. MENGES and F. KNIPSCHILD, *Polym. Engng Sci.* **15** (1975) 623.
4. L. J. GIBSON and M. F. ASHBY, *Proc. Roy. Soc. Lond.* **A382** (1982) 43.
5. S. K. MAITI, L. J. GIBSON and M. F. ASHBY, *Acta Metall.* **32** (1984) 1963.
6. A. G. GENT and A. N. THOMAS, *J. Appl. Polym. Sci.* **1** (1959) 107.
7. *Idem, Rubber Chem. Technol.* **36** (1963) 597.
8. S. K. MAITI, M. F. ASHBY and L. J. GIBSON, *Scripta Metall.* **18** (1984) 213.
9. L. J. GIBSON and M. F. ASHBY, "The Structure and Properties of Cellular Solids" (Pergamon Press, Oxford, 1988).
10. F. K. ABD EL SAYED, R. JONES and I. W. BURGESS, *Composites* **10** (1979) 209.
11. L. J. GIBSON, M. F. ASHBY, G. S. SCHAJER and C. I. ROBERTSON, *Proc. Roy. Soc. Lond.* **A382** (1982) 25.
12. T. P. HARRIGAN and R. W. MANN, *J. Mater. Sci.* **19** (1984) 761.
13. S. V. KANAKKANATT, *J. Cell. Plast.* **9** (1973) 50.
14. B. S. MEHTA and E. A. COLOMBO, *ibid.* **12** (1976) 59.
15. A. CUNNINGHAM, *Polymer* **22** (1981) 882.
16. N. C. HILYARD (ed.), "Mechanics of Cellular Plastics" (Applied Science, London, 1982).
17. K. I. MAL'TSEV, *J. Sov. Phys. Acoustics* **13** (1968) 391.
18. M. R. PATEL, PhD thesis, University of California at Berkeley, California, USA (1969).
19. S. GUPTA, B. WATSON, P. W. R. BEAUMONT and M. F. ASHBY, Final Year Project, Cambridge University Engineering Department, Cambridge, UK (1986).
20. J. R. DAWSON and J. B. SHORTALL, *J. Mater. Sci.* **17** (1982) 220.

Received 21 September 1987
and accepted 11 January 1988